Title
A three-dimensional approach to mitotic chromosome structure: evidence for a complex hierarchical organization.

Permalink
https://escholarship.org/uc/item/51d5h5vr

Journal
Journal of Cell Biology, 105(1)

ISSN
0021-9525

Authors
Belmont, AS
Sedat, JW
Agard, DA

Publication Date
1987-07-01

DOI
10.1083/jcb.105.1.77

Peer reviewed

A Three-dimensional Approach to Mitotic Chromosome Structure: Evidence for a Complex Hierarchical Organization

Andrew S. Belmont, John W. Sedat, and David A. Agard

Department of Biochemistry and Biophysics and the Howard Hughes Medical Institute,
University of California, San Francisco, California 94143-0448

Abstract. We describe findings on the architecture of *Drosophila melanogaster* mitotic chromosomes, made using a three-dimensional–oriented structural approach. Using high-voltage and conventional transmission electron microscopy combined with axial tomography and digital contrast-enhancement techniques, we have for the first time visualized significant structural detail within minimally perturbed mitotic chromosomes. Chromosomes prepared by several different preparative procedures showed a consistent size hierarchy of discrete chromatin structural domains with cross-sectional diameters of 120, 240, 400–500, and 800–1,000 Å. In fully condensed, metaphase-arrested chromosomes, there is evidence for even larger-scale structural organization in the range of 1,300–3,000-Å size. The observed intrachromosomal arrangements of these higher-order structural domains show that both the radial loop and sequential helical coiling models of chromosome structure are oversimplifications of the true situation. Finally, our results suggest that the pathway of chromatin condensation through mitosis consists of concurrent changes occurring at several levels of chromatin organization, rather than a strictly sequential folding process.

THE principle underlying mitotic chromosome organization is at present unknown, reflecting the difficulties associated with investigations into chromosome structure. First, chromatin is extremely sensitive to changes in its environment: the ionic strength, divalent cation concentration, pH, mechanical shear forces, and presumably as yet unidentified factors. It is likely that this in vitro sensitivity reflects the tremendous plasticity observed in chromosome structure in vivo during normal cell cycle progression. Experimentally, this sensitivity to environmental conditions has meant different investigators often have studied essentially different objects. Second, mitotic chromosomes have a very high packing ratio combined with a high structural complexity; typically 50,000 μm of DNA is folded reproducibly yet nonsymmetrically into a chromosome 5 μm long. Third, and perhaps most significantly, mitotic chromosomes are too small for optical microscopy to provide significant structural detail, but still too large for conventional electron microscopic approaches.

In the past, investigators have dealt with these difficulties mostly through approaches aimed at reducing the overall complexity of the problem. This has meant either employing various extraction procedures designed to progressively unfold the chromosome (4, 5, 9, 16, 19–23, 25, 38, 41), or focusing on particular features of chromosome structure, such as surface topology (7, 14, 19, 35) or recognized size regularities as seen in certain views (29, 31, 41), and then extrapolating these features to the simplest model compatible with such observations. Although much useful information

has come from such studies, they did not allow the determination of the organization of native chromosomes. Thus, the inherent contradictions between two current models of chromosome structure, the radial loop model (1, 9, 19, 25) and a model involving successive helical coiling (5, 31), illustrate the insufficiencies of these approaches.

To avoid these problems, we have concluded that a three-dimensional reconstruction will be required to determine even basic features of the architecture of chromosomes in their native, compact conformation. To accomplish such a reconstruction, we have used electron microscopy combined with axial tomography and various image-enhancement techniques to study *Drosophila melanogaster* mitotic chromosomes prepared using several different procedures. We present here the results of several reconstructions, as well as the analysis of numerous stereo pairs covering a 120° angular range. Our findings allow the following conclusions.

The vast majority, if not all, of the chromosome, is made up of a basic fiber, roughly 100–140 Å in diameter. This basic fiber is organized in complex but characteristic folding patterns, giving rise to distinct higher-order structural domains measuring 220–260, 400–500, and 800–1,000 Å in diameter, respectively. Evidence for even larger-scale structural organization in the 1,300–3,000-Å range is present in the fully condensed metaphase-arrested chromosomes. Although the exact folding patterns giving rise to these structural domains have not yet been determined, it is clear that a much larger-scale organization of chromatin exists within mitotic chromosomes than was appreciated in many earlier electron

microscopy investigations. Finally, the intrachromosomal arrangement of these higher-order structural domains is such that both the radial loop and the sequential helical coiling models of chromosome structure are shown to be oversimplifications of the true situation.

Materials and Methods

Isolation of Embryonic Chromosomes

Drosophila melanogaster, Oregon R stock embryos were obtained from population cages. Collection periods of 1–2.5 h were used, with harvesting carried out 3 h after the start of collection to ensure that embryos would be at syncytial blastoderm or earlier in developmental stage (11). Embryos were harvested, washed, and dechorionated according to standard procedures (10).

Embryos were washed and suspended in cold chromosome isolation buffer, buffer A (80 mM KCl, 20 mM NaCl, 0.5 mM EGTA, 2 mM EDTA, 15 mM Pipes buffer [ph 7.0], 15 mM β-mercaptoethanol, 0.5 mM spermidine, 0.2 mM spermine, 10 µg/ml turkey egg white protease inhibitor [Sigma Chemical Co., St. Louis, MO]), and physically disrupted either by using 10 strokes of a Dounce homogenizer (producing individual chromosomes and intact nuclei) or by gentle squashing (producing intact mitotic plates). Previous studies have shown that buffer A preserved polytene chromosome structure, as assayed by maximization of birefringence in polarization microscopy, better than other commonly used chromosome isolation buffers (31).

Isolated chromosomes were obtained through a slight modification of the method of Blumenthal et al. (6). Digitonin and Brij 58 were added to final concentrations of 0.1% and 0.17%, respectively, the suspension was filtered through a 100-µm mesh nylon sieve, and ~10 ml of the suspension was placed in a 50-ml conical centrifuge tube and vortexed for 2 min.

The crude chromosome preparation was layered on top of a 24-ml 10–50% (wt/vol) sucrose gradient (in buffer A), and spun at 10,000 rpm for 1 h at 4°C using a SW27 rotor (Beckman Instruments, Inc., Fullerton, CA). Chromosomes and nuclei pelleted to the bottom of the gradient.

All of the above operations were carried out at 4°C.

Fixation and Critical Point Drying of Isolated Embryonic Chromosomes

Formvar-coated (1.5%) titanium 100-mesh EM grids were carbon-coated on the reverse side; a 0.02% poly-L-lysine solution (540 kD molecular mass, Sigma Chemical Co.) was used to coat the formvar surface, and colloidal gold beads (37) ~500 Å in diameter were applied to this surface.

10 µl of the chromosome-nuclear fraction from the sucrose gradient, resuspended in buffer A, was applied per grid. After incubation for 1–2 h at 4°C, grids were transferred to a 3:1 (vol/vol) solution of buffer A/8% glutaraldehyde (Polysciences, Inc., Warrington, PA), and fixation was carried out overnight at 4°C.

After fixation the grids were washed in cold buffer A, and dehydrated at 0°C using an EtOH series of 10% increments (buffer A used to 60% EtOH, then ddH₂O). Critical point drying (CPD)[1] was carried out using a Sorvall apparatus (DuPont-Sorval, Newtown, CT) and liquid CO₂. Grids were transferred immediately after CPD to a vacuum desiccator.

Preparation of Intact Embryos for Embedding

Fixation and hand dissection of the vitelline membranes were carried out according to the method of Zalokar and Erk (40). Dechorionated embryos rinsed in buffer A were immersed for 6 min in a heptane solution which had been preequilibrated with an equal volume of buffered 7.3% glutaraldehyde solution. Embryos were then transferred into buffer A and the vitelline membranes were dissected off using a sharpened tungsten needle.

In an attempt to reduce the background nucleoplasm staining (32, 33), devitellinized embryos were incubated for 2 h in buffer A supplemented with 0.1% digitonin, 0.17% Brij 58, and 50 µg/ml of heat-treated pancreatic RNase, washed with buffer A, and fixed further in a 3:1 mixture of buffer A/8% glutaraldehyde at 4°C overnight. In a minority of embryos this treat-

---

1. *Abbreviations used in this paper:* CPD, critical point drying; HVEM, high-voltage electron microscopy.

ment produced significant extraction, increasing the chromosome contrast, although this effect was usually over only a portion of the embryo.

Dehydration before embedding was carried out using the same protocol described above for CPD of the isolated chromosomes.

Isolation of Chromosomes from Kc Cells

Cells were grown at 24°C in Falcon 75-cm² flasks (Falcon Labware, Oxnard, CA) using Eschalier medium. For chromosome preparations, cells from 10 75-cm² flasks were treated with 2.5 µg/ml Colcemid (Sigma Chemical Co.) for 1.5 h or with 0.5 µg/ml Colcemid for 4 h, then harvested by shaking free the loosely attached cells. Cells were pooled, pelleted for 5 min at low speed at 4°C, resuspended in cold chromosome isolation buffer, pelleted again under the same conditions, and resuspended in ~8 vol of cold chromosome isolation buffer.

For chromosome isolation a cell suspension in buffer A was supplemented with digitonin and Brij 58 (concentrations as above) plus 0.5 mM phenylmethylsulfonyl fluoride (PMSF); vortexing yielded a mixture of chromosome clusters and isolated chromosomes depending on the duration of vortexing. This chromosome suspension was layered on a multistep sucrose gradient (5.5 ml 82%, 5.5 ml 70%, 5.5 ml 60%, 5.5 ml 50%, 4 ml 40%, 4 ml 20%) containing 0.5 mM PMSF, and spun as described above. Chromosome clusters and nuclei were found at the 82–70% interface, isolated chromosomes, small chromosome clusters, and nuclei at the 70–60% interface, and mostly isolated chromosomes at the 60–50% interface. All steps were carried out at 4°C.

Before embedding, fractions from the various sucrose gradient interfaces were removed and 8% glutaraldehyde was slowly added to a 2% final concentration. Fractions were further diluted with 2 vol of a 3:1 buffer A/8% glutaraldehyde solution and chromosomes were pelleted briefly in a Microfuge (Beckman Instruments, Inc.). Fixation was carried out in the 3:1 buffer A/8% glutaraldehyde solution overnight at 4°C. Dehydration was carried out as described for the CPD procedure.

Embedding, Sectioning, and Section Staining

Samples were embedded in Epon 812 using a standard formulation and infiltration schedule (15), and sections 0.1–1.0 µm thick were cut. Grids were immersed for 25 min in a 50% EtOH solution that contained 0.2% uranyl acetate, to stain the sections from both sides. They were poststained from both sides in 0.02% lead citrate. Poly-L-lysine and gold beads of diameter 140–200 Å were applied to both surfaces of the sections, as described earlier. Before data collection, sections were carbon-coated on one surface.

Microscopy and Data Collection

CPD embryonic chromosomes were examined using the 1500-kV Kratos/AED high-voltage electron microscope (Kratos Analytical Instruments, Ramsey, NJ) located in the Materials Science division of the Lawrence Berkeley laboratories. The 35-µm objective aperture was used and focusing was accomplished by the method of minimum contrast. Magnification routinely was between 8,000 and 10,000. A specially built stage allowed tilt angles from +60° to −60°. Data sets for axial tomography reconstructions consisted of pictures at 5° intervals from +60° to −60° tilt. Kodak SO-163 sheet film was used; all negatives from a data set were developed together at 68°F for 4 min in fresh Kodak D-19 developer (Eastman Kodak Co., Rochester, NY).

Sections 1,200–2,000 Å thick were viewed in a Philips 400 microscope (Philips Electronic Instruments, Inc., Mahwah, NJ) operated routinely at 100 or 120 kV; data sets were all collected at 120 kV, and at 15,200 magnification. Slight modification of the normal Philips EM400 stage allowed tilt data sets of ±60° to be collected from the central region of the grid. To minimize section shrinkage during data collection, sections were preirradiated by exposure to the electron beam for 10 min at an intensity corresponding to roughly a 1 OD film density with a 2-s exposure (15,200 magnification); during actual data collection a low dose box was used to limit exposure between pictures. Tilt sets were from ±60° in 5° intervals. Kodak EM 4489 film was used with D-19 developer as described above.

Scanning Densitometry and Mass Normalization

Negatives were scanned on a Syntex AD1 microdensitometer (Nicolet Instrument Corp., Madison, WI) (30). A square scanning aperture of 32 × 32 µm² was used with a 32-µm scanning increment. Kodak Wratten gelatin neutral density filters between 0.3 and 0.6 OD were used as calibration

standards to allow OD offsets of background, so that measurements could be made within the linear range of the AD1 and at maximum sensitivity. An unexposed film, developed in parallel with each data set, was scanned to establish the film fog level.

The corrected OD value at a given picture element (pixel) was given by the following equation: $OD_{pixel} = OD_{measured} + OD_{offset} - OD_{fog}$. For axial tomographic reconstruction, it is necessary to convert these corrected film OD values into values proportional to the integrated scattering cross section, or electron optical density. Assuming the electron intensity to be proportional to the corrected OD, the electron OD of the projected image at a given pixel is calculated as $-\log(OD_{pixel}/OD_{background})$; the background OD is calculated from the mode of the corrected OD values in a region surrounding the chromosome in each projection.

Data Set Alignment and Axial Tomography Reconstruction

Because of x-y image plane rotations and translations, as well as possible small changes in magnification, the projected images of a given data set must be computationally aligned, using the projected positions of the gold beads in the neighborhood of the object of interest as fiducial marks. We used a procedure (18) based on a least squares estimator and a conjugate gradient minimization algorithm to solve for a common tilt axis, relative magnification changes, x-y rotational and translational offsets, the actual tilt angle of each projection, and the three-dimensional positions of the beads. Our numerical simulations demonstrated that by using eight or more beads, tilt angles >10° could be calculated to an accuracy of <0.5°, changes in magnification to within 0.5%, and x-y rotation offset angles to an accuracy of roughly 0.2°, when beads were distributed over an x-y planar surface. When beads are placed at varying z height, as when coated on both sides of a plastic section or distributed over a nonplanar surface (i.e., a nonflat formvar surface), significant improvements in parameter determination are obtained, particularly for tilt angle determination at lower angles. Actual image alignment was carried out using quadratic interpolation.

Three-dimensional reconstructions were obtained through a series of two-dimensional axial tomography reconstructions. We used an R-weighted back projection algorithm (13, 27) carried out in Fourier space with the addition of a gaussian roll-off frequency filter.

Resolution of Reconstruction

In estimating the resolution of the three-dimensional reconstructions, the following considerations were taken into account. The actual three-dimensional reconstruction is obtained as a series of two-dimensional axial tomography reconstructions, carried out in a plane perpendicular to the tilt axis. Parallel to the tilt axis, the resolution of the final three-dimensional reconstruction is limited only by the resolution of the original micrographs and the accuracy in aligning the negatives. Given n projections distributed equally over the entire angular range, a very stringent resolution estimate for the two-dimensional reconstruction resolution is given by $R = 2\pi d/(n + 3)$, where d is the specimen radius (17). This corresponds to roughly 330 Å in the reconstruction of the CPD chromosome and 170 Å in the reconstruction of the embedded anaphase mitotic plate. By the Rayleigh criterion, a Fourier resolution of 330 Å (170 Å) implies that objects of 200 Å (100 Å) can be resolved. Data beyond this resolution were eliminated using a gaussian cutoff to minimize series termination ripples. Although not strictly necessary, the data were also filtered along the y (tilt) axis to reduce the apparent spatial nonuniformity of resolution.

The result of incomplete angular sampling (only ±60° observed) is a decreased resolution, or blurring in the z direction of the reconstruction (2) (where the x-y plane of the reconstruction corresponds to the projection plane at zero tilt), which also must be considered in the interpretation of the reconstruction.

Although it is difficult to establish an exact resolution limit, we feel the limited conclusions summarized in the Results section are justified. Namely, although the reconstructions were not of sufficient resolution to actually trace individual 120-Å fibers over extended distances in three dimensions, they did show the same size structural domains as recognized in the original projections, however, now visualized as distinct, spatially defined entities in three dimensions.

Local Contrast-Image Enhancement

Local contrast enhancement was accomplished based on a recently described general algorithm (26). First the local mean intensity in an appropri-
ate size box surrounding a given pixel is calculated; then the local contrast, defined by the increment in intensity of this pixel relative to the local mean intensity, is calculated. Using a continuous, piecewise linear transformation, tailored by the user for the particular image to be enhanced, the initial local mean intensity is mapped to a new value. Similarly, a new local contrast is also calculated by multiplying the original local contrast by a factor whose value is based on a continuous, piecewise linear function of the original local mean intensity. The new local mean and local contrast values then are added to give the transformed intensity level for the given pixel. This procedure repeated over all pixels of the image, with modifications for the image border, yields the final enhanced image.

Results

CPD Chromosomes: High-voltage EM and Image Enhancement

We first investigated the structure of isolated, intact mitotic chromosomes from syncytial blastoderm embryos. A requirement of axial tomography is that a true projection of the specimen be obtained. This requires use of a high-voltage electron microscope (HVEM), which not only enables the entire specimen (typically covering several micrometers depth of field) to be viewed simultaneously in focus, but also significantly reduces the electron scattering cross section, allowing thick specimens to be examined with minimal multiple scattering and chromatic aberration effects (12).

We initially chose to prepare samples by critical point drying in an effort to compensate for the lower contrast of HVEM images and the inherently low internal contrast of the highly condensed mitotic chromosomes. Even with the use of CPD specimens, however, the large dynamic range of gray levels combined with the low contrast present within the chromosome obscured the actual information content of the micrographs.

In order to develop an effective means of visually extracting information from the images, various image-enhancement methods were explored. A local contrast-enhancement technique based on a recently described general algorithm (26) proved the most useful. Fig. 1 demonstrates the use of this method, showing both an original and local contrast-enhanced stereopair of a CPD chromosome. A substantial increase is apparent in the clarity with which individual component fibers stand out visually, down to 120-Å nucleofilaments. Careful comparison demonstrates that all features recognized in the enhanced images can be found in the original unenhanced images; the local enhancement procedure does not introduce additional spurious structures. Extensive use of this procedure will be made to display results throughout this paper.

Overall Chromosome Morphology

A large number of CPD chromosomes were studied and several complete tomographic data sets were collected. In all cases the chromosomes had the same general appearance. Figs. 1–5, described below, show several examples chosen to illustrate features observed consistently in all CPD chromosomes examined to date.

Chromosomes isolated by our procedures are generally compact in appearance, in marked contrast to a number of previously published EM reports showing large numbers of extruded 120- or 300-Å fibers extending for long distances from the border of isolated chromosomes. Typically, the maximum cross-sectional diameter ranges from 0.35 to 0.55
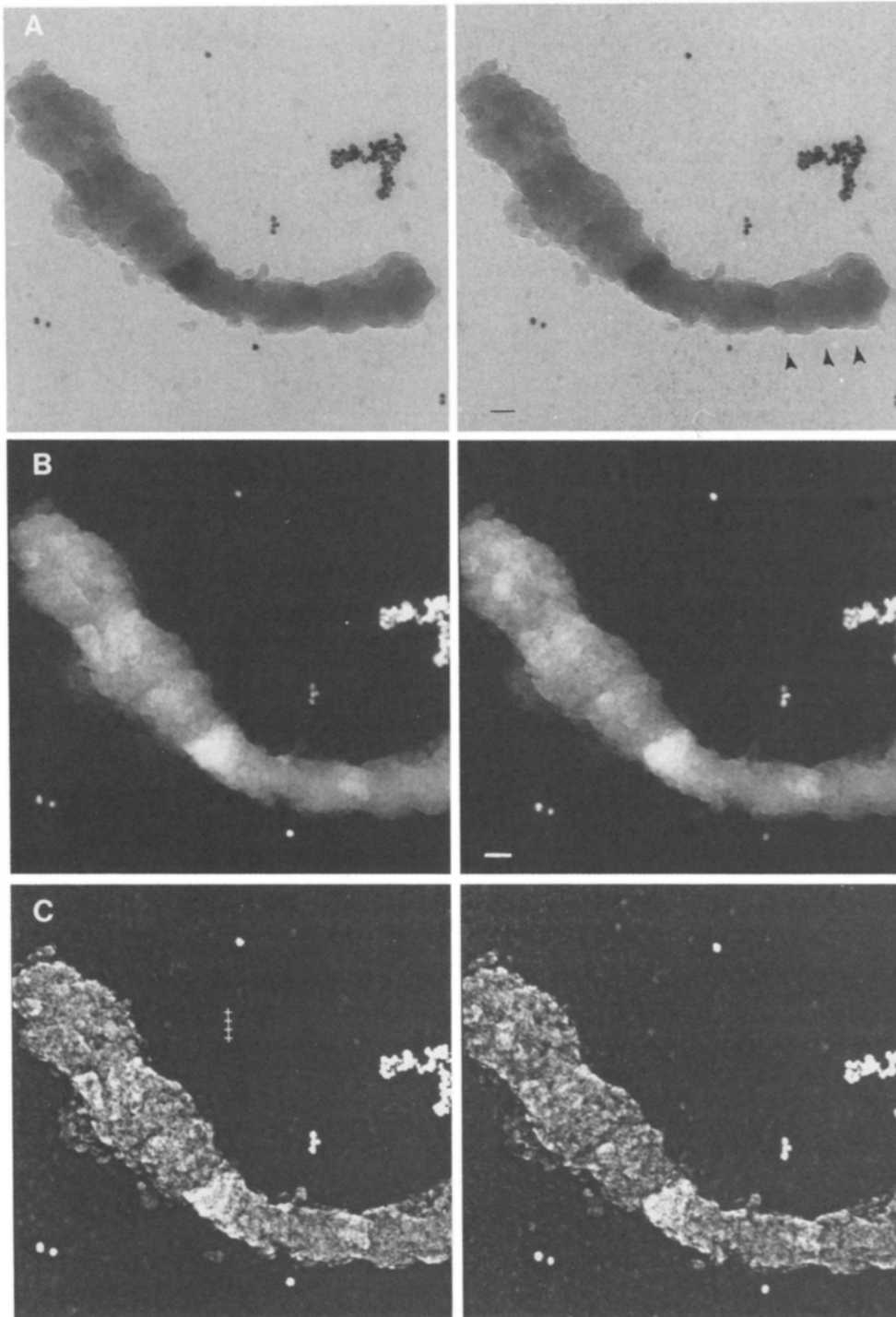
Figure 1. A typical stereopair of a CPD chromosome imaged at 1.5 MeV is presented; tilt angles are +55° and +50°, with the tilt axis oriented vertically. (*A*) Prints made directly from the HVEM negatives. Note the compact appearance and smooth borders over most of the chromosome, with an absence of extruding fibers, indicative of structural preservation. Grooves in the chromosome border delineating several contiguous chromatin blocks are marked by *arrowheads*. (*B*) "Mass normalized" digitized images displayed on a 512 × 512-pixel, 256 gray scale monitor in which the brightness at each pixel is proportional to the electron scattering from the projected path through that pixel. (Unless specified otherwise, all of the remaining figures in this paper represent digitized images photographed in this manner.) (*C*) Same digital image as in *B* after local contrast enhancement based on a box size of 21 × 21 pixels (672 × 672 Å). A significant increase in the clarity of individual component fibers is apparent in the enhanced image. All features recognized in *C* can be recognized in retrospect in *A* and *B*. Bar (*A* and *B*), 1,000 Å. Crosses (*C*), separated by 320 Å (10 pixels). Pixel size (*B* and *C*), 32 Å.

μm, with the minimum diameter roughly one-half this thickness. Based on stereoviews, the chromosomes are interpreted as consisting of two daughter chromatids, seen either lying parallel but closely abutted (Fig. 1) or else loosely coiled about each other (Figs. 2 and 3). Thus the diameter of the individual chromatids measures ∼0.2 μm. This is considerably less condensed than the 0.4–0.6-μm chromatid diameter observed for the majority of the Colcemid-blocked Kc metaphase chromosomes, but comparable to the chromatid diameters observed in sections of anaphase mitotic plates in embryos.

Chromatid Substructure: Evidence for Discrete Size Structural Domains

The lowest-order structural entity recognized measured 3–4 pixels in width, as seen in Figs. 2 and 3, where the pixel size is 40 Å; presumably this corresponds either to a 120-Å polynucleosome filament or possibly a face-to-face stacking of nucleosomes in a higher-order chromatin fiber as predicted in folded-ribbon or two-start helical models (3, 39). This size fiber we observed almost exclusively within larger-size structural domains, in which a regular cross-striation pattern of
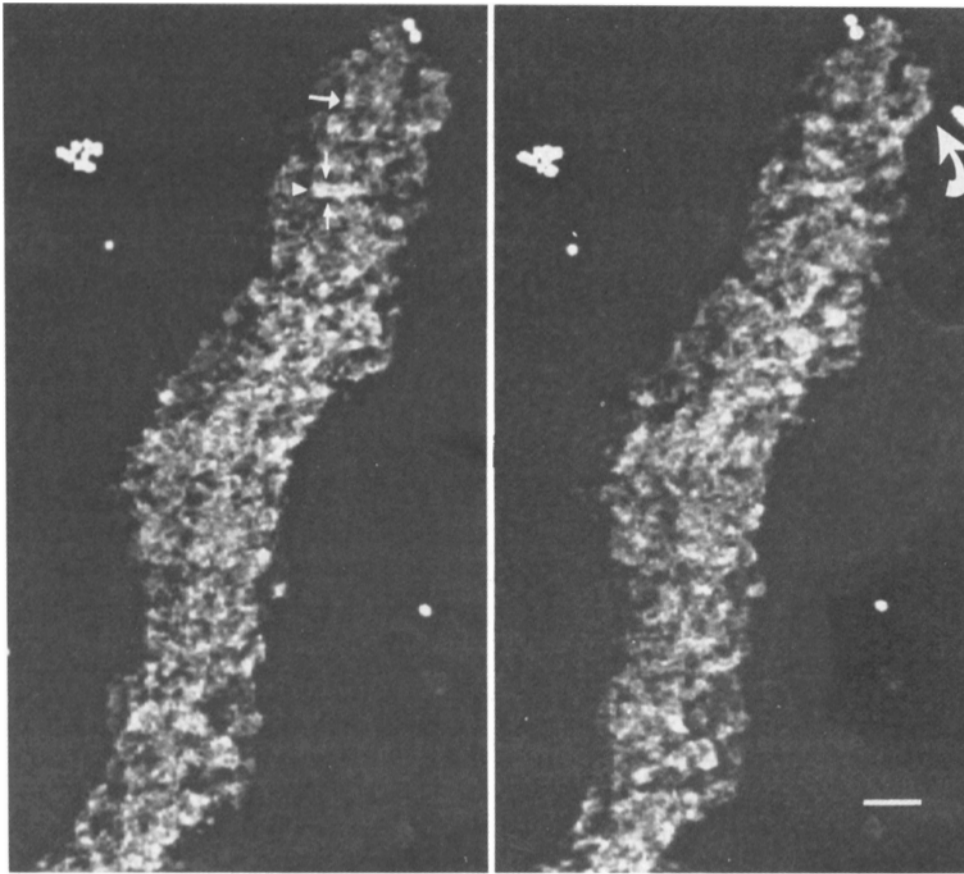
Figure 2. Stereopair of another CPD chromosome; 10° of tilt separate each view. Local-contrast enhancement with a box size of 21 × 21 pixels (840 Å) was used. *Arrow* marks 120-Å cross striations visualized within both 240- and 400–500-Å-diam higher-order structures. *Arrowhead* points to 400–500-Å structural domain (see also Fig. 3) further delineated by *small arrows.* Note the flattened, elliptical profile of the looping 400–500-Å fiber marked by *large, curved arrow.* Bar, 1,200 Å. Pixel size, 40 Å.

120 Å was frequently seen (indicated by *small arrows* in Figs. 2 and 3). We therefore conclude that the vast majority of chromatin within mitotic chromosomes is present within higher-order chromatin structures, 240 Å and larger in diameter.

The most conspicuous higher-order structures recognized in these electron micrographs were 400–500-Å linear structural domains, or "fibers," seen largely as running diagonally or perpendicular to the chromosome axis, or as peripheral loops (Fig. 2, *curved arrow*). As mentioned above, they frequently showed cross striations of ~120 Å in spacing. Less frequently, cross striations of ~240 Å were seen within these 400–500-Å domains; in the example shown in Fig. 3 the cross striations present in one view of a 400-Å domain are 240 Å, but are 120 Å in a neighboring view, separated by 10° of tilt.

When observed in stereoviews, these 400-Å "fibers" sometimes gave the impression of being flattened ribbons, with elliptical cross sections 400–500 Å in diameter in one direction, but considerably less in the orthogonal direction (see peripheral loop in Fig. 2). This impression was supported by examples in which the same "fiber" or domain appeared 400–500 Å in diameter in one projection, but roughly 240 Å in an adjacent projection (see *small arrowhead with dash* in Fig. 3). In certain cases, though, a different impression of two ~240-Å fibers running parallel to create an apparent discrete 400–500-Å-diam structure was obtained.

Separate fibers 240 Å in diameter that appear unrelated to the 400–500-Å domains were also visualized. Also recognizable, but not nearly as prominent as the 400–500-Å do-

mains, were regions roughly 800–1,000 Å in diameter (indicated by *large arrow heads* in Fig. 3). In these CPD embryonic chromosomes, these regions were less distinct than the 400–500-Å structural domains, but could be recognized in some regions of nearly all the chromosomes we analyzed.

In contrast, as will be discussed later, in metaphase-arrested chromosomes these observations are reversed, with the 800–1,000-Å structures being more prominent than the 400–500-Å structural domains.
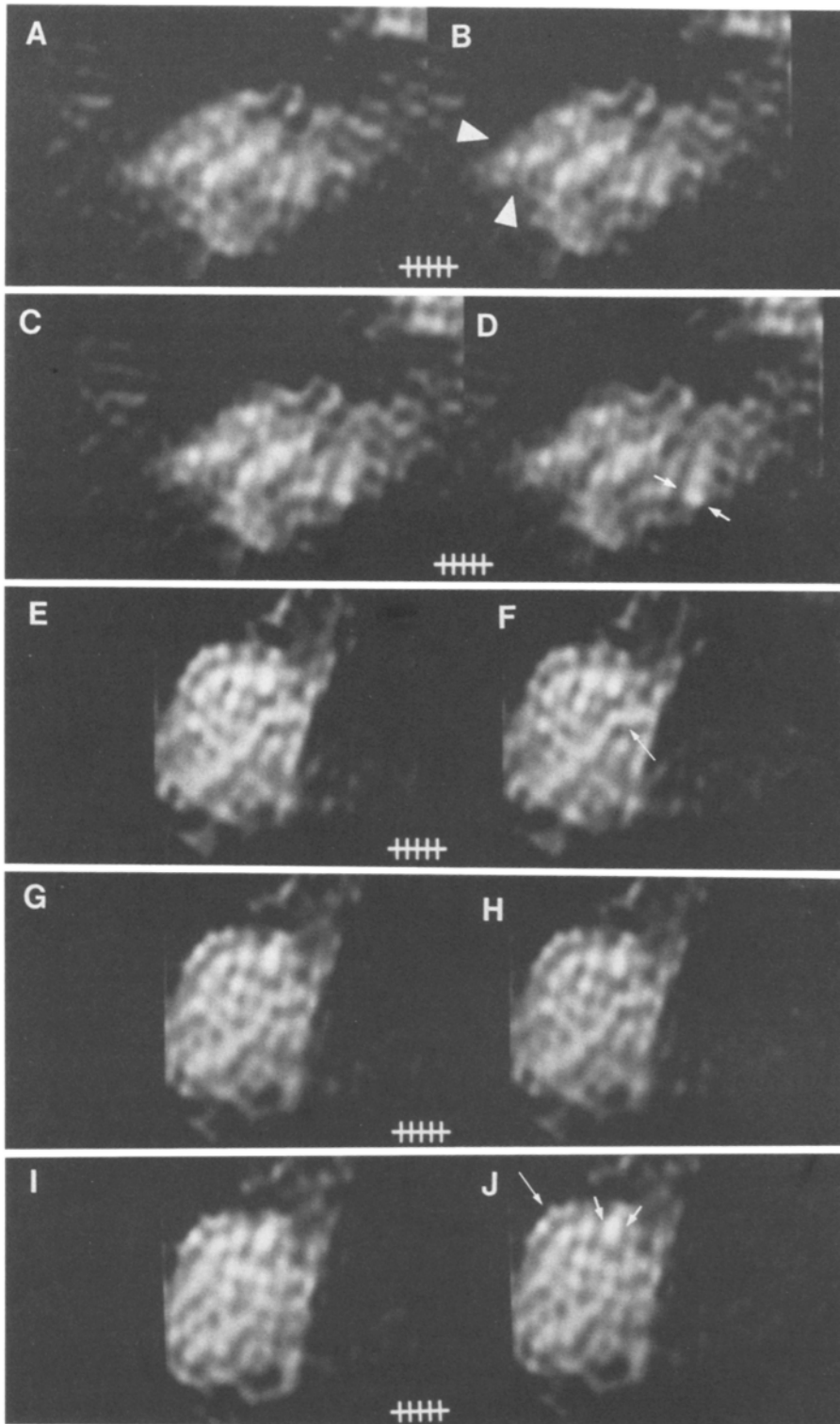
Axial Tomography Reconstruction

Further support for the existence of discrete sized higher-order chromatin domains was provided by an axial tomography three-dimensional reconstruction of a region of the chromosome shown in Fig. 3. The reconstruction was based on 23 views covering ±60°, with 5° intervals between views (except for two projections which could not be aligned correctly, resulting in tilt intervals of roughly 10°.

Fig. 4 shows selected slices from this reconstruction, chosen to best illustrate certain common structural features. The three-dimensional reconstruction was rotated such that the chromosomal axis would be roughly perpendicular to the displayed reconstruction sections. Fig. 4, *A–D* represents consecutive sections, spaced 40 Å (1 pixel) apart. A roughly 800–1,000-Å-diam structural domain, or "fiber," is seen at the top of the sections and is delineated in Fig. 4 *B* by *large arrowheads.* Delineated by *arrows* in Fig. 4 *D* is a roughly 400-Å diam domain.
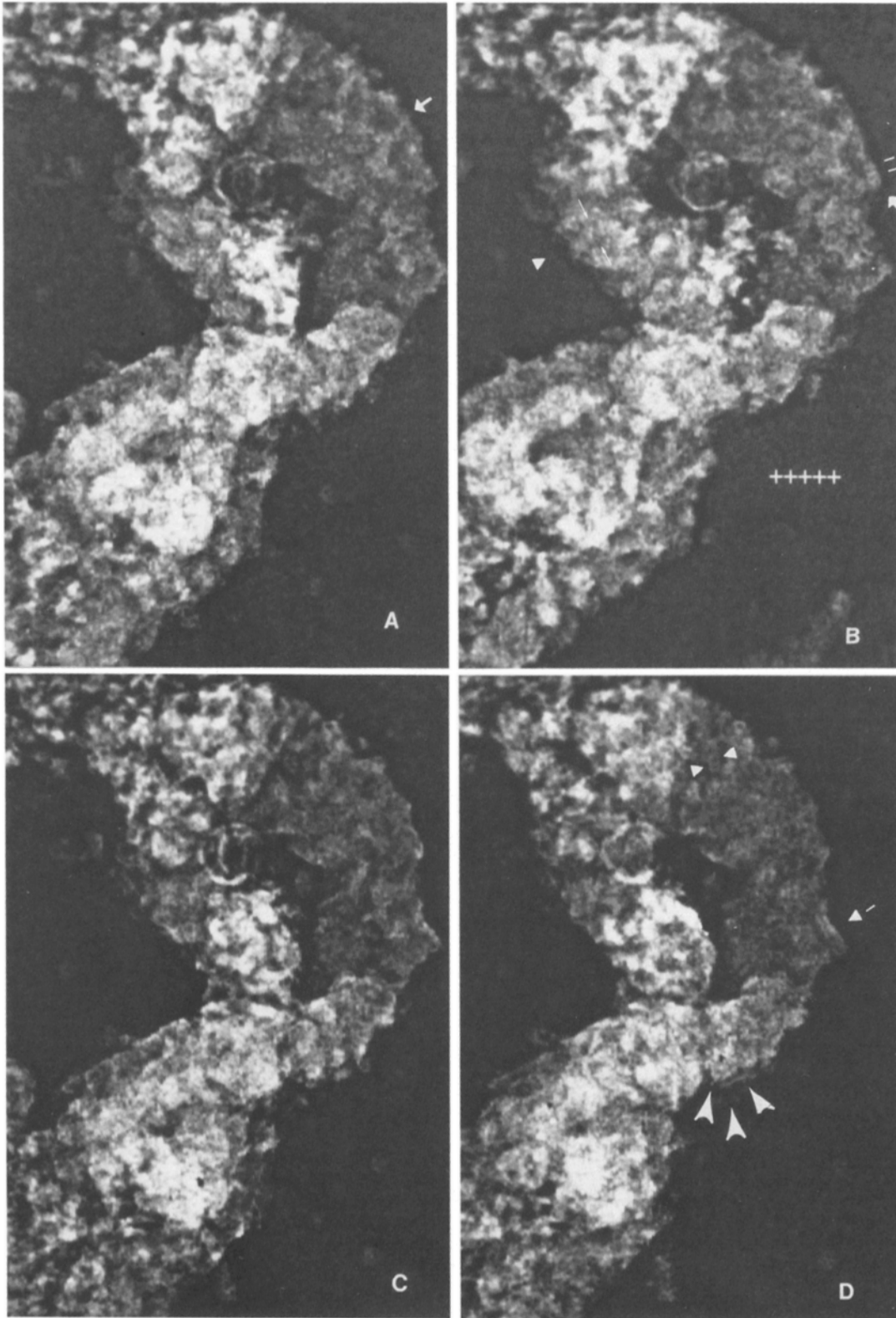
Figure 3. Enhanced stereopairs of a different CPD chromosome, tilt angles (*A*) +60°, (*B*) +50°, (*C*) +45°, (*D*) +40°. *Arrows* mark 120-Å cross striations in higher-order structures; *small arrowheads* (*B, D*) mark 400–500-Å-diam structural domains, further delineated in *B* by *thin arrows*; *small arrowhead with dash* (*D*) marks "fiber" appearing 400–500 Å in diameter in *D* but 240 Å in *C*. *Parallel dashes* mark feature with roughly 120-Å cross striations in *B*, 240 Å in *A*. *Large arrowheads* (*D*) mark 800–1,000-Å domain. Crosses separated by 400 Å (10 pixels).

Figure 4. Selected slices of a tomographic reconstruction for the CPD chromosome displayed in Fig. 3. Two consecutive two-dimensional rotations, in different planes, were carried out on the reconstruction to place the chromosomal axis roughly perpendicular to the reconstruction slices. *(A–D)* Consecutive sections, spaced 40 Å apart (1 pixel). *Arrowheads* point to 800–1,000-Å structural domains, *pairs of arrows* delineate a 400-Å-diam structural domain. *(E–J)* Consecutive reconstruction slices, 40 Å apart, from a region roughly 0.22 µm distant to that shown in *A–D. Long, thin arrows* point to fibers, roughly 240 Å in diameter. *Short arrows* outline a region 400 Å wide. Crosses separated by 200 Å (5 pixels).

Fig. 4, *E–J* represents consecutive sections from a region roughly 0.22 µm distant from that shown in Fig. 4, *A–D*. Although structural domains of 800–1,000 Å are not visible here, in several cases fibers of ∼240 Å in diameter can be visualized, as indicated by *arrows* in Fig. 4, *F* and *J*. Certain areas of these sections are consistent with the existence of 400–500-Å domains, but given the quality of the reconstruction in these areas distinct structural domains can not be delineated.

In Fig. 5, rather than showing consecutive sections, stereopairs calculated from short stacks of sections from the tomographic reconstruction are displayed. In this case, both
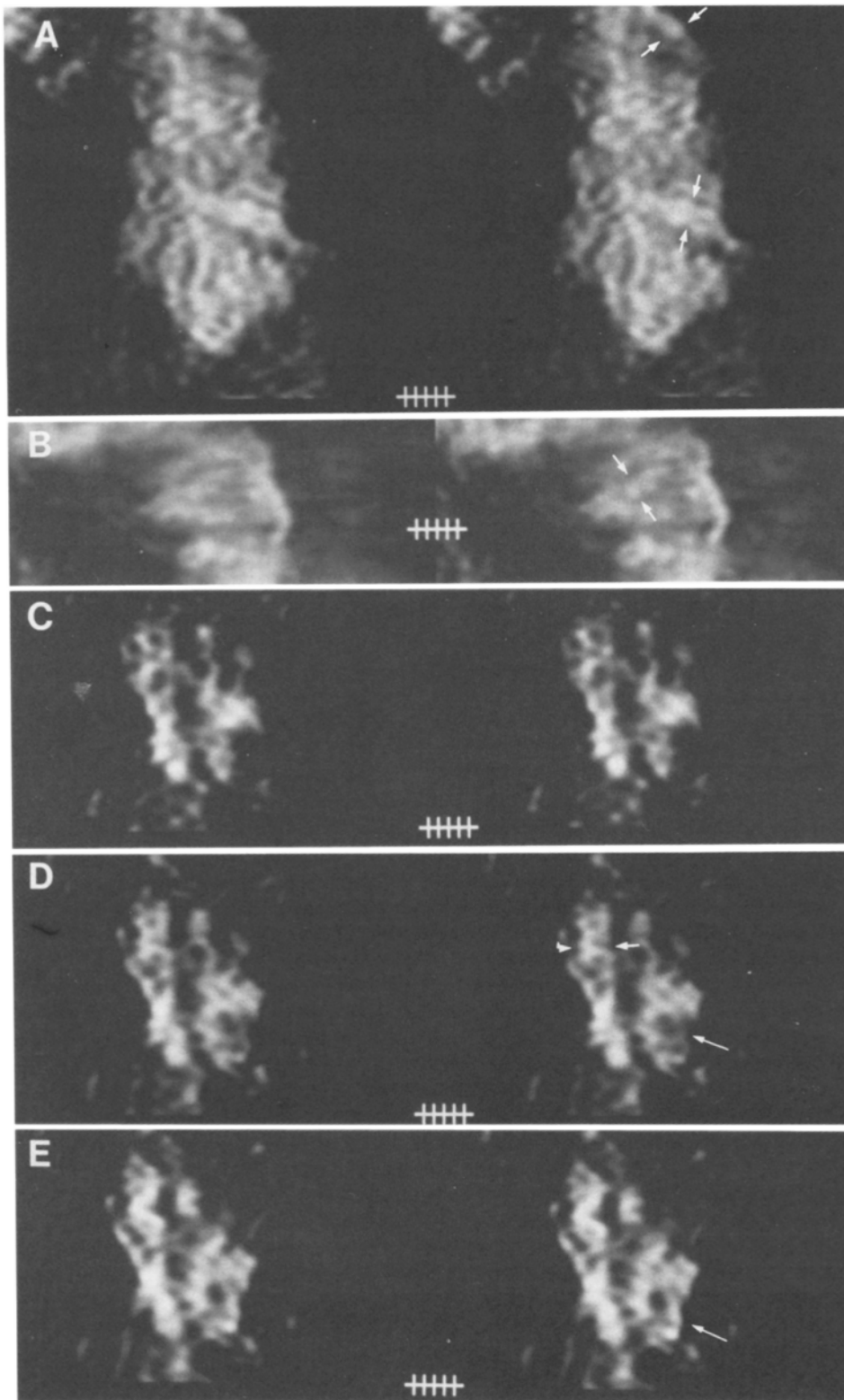
Figure 5. Stereopairs of short stacks are shown here from the same tomographic reconstruction as displayed in Fig. 4. Short stacks of reconstruction slices have been rotated computationally ±6° about an axis parallel to the vertical axis of the figure, and the intensity values from the rotated stacks projected onto the plane of the figure. The reconstruction has been "sliced" in sections perpendicular to the z-axis (the projection axis at zero tilt), with the vertical axis corresponding to the original tilt axis. These reconstruction slices therefore more closely correspond to longitudinal chromosome sections rather than the transverse sections of Fig. 4. (*A*) Calculated using a 480-Å-thick stack (12 sections). Because the chromosome axis is actually curved in the y-z plane, the bottom of *A* corresponds to a region where the chromosome is bending into the plane of the figure. *Arrows* outline 400–500-Å-diam "fibers." (*B*) From a stack 520 Å thick; note the roughly 400–500-Å-diam "fiber" looping across the chromatid, marked by *arrows*. (*C–E*) From a set of sequential, overlapping stacks 280 Å thick; going from *C* to *D* and from *D* to *E* represents steps of 120 Å deep through a region that just grazes the surface of the chromosome. *Longer arrows* point to a 400–500-Å fiber forming a loop. *Shorter arrows* outline a roughly 800-Å-diam structural domain. Crosses separated by 200 Å (5 pixels).

240–280- and 400–500-Å-diam elements can be visualized as spatially discrete entities in three dimensions. In Fig. 5, *C–E*, an 800-Å-diam feature is recognized as well.

Embedded Embryos: Anaphase Mitotic Plates

To determine whether the structural features observed in CPD embryonic chromosomes were also seen using a differ-

ent preparation scheme, 1,500–2,000-Å Epon sections of mitotic plates were examined. A precellular blastoderm embryo synchronized in anaphase was chosen; this eliminated the additional complexity created by the intertwining of daughter chromatids, seen in the CPD chromosomes of syncytial blastoderm embryos.

The precellular blastoderm chromosomes, present as sin-
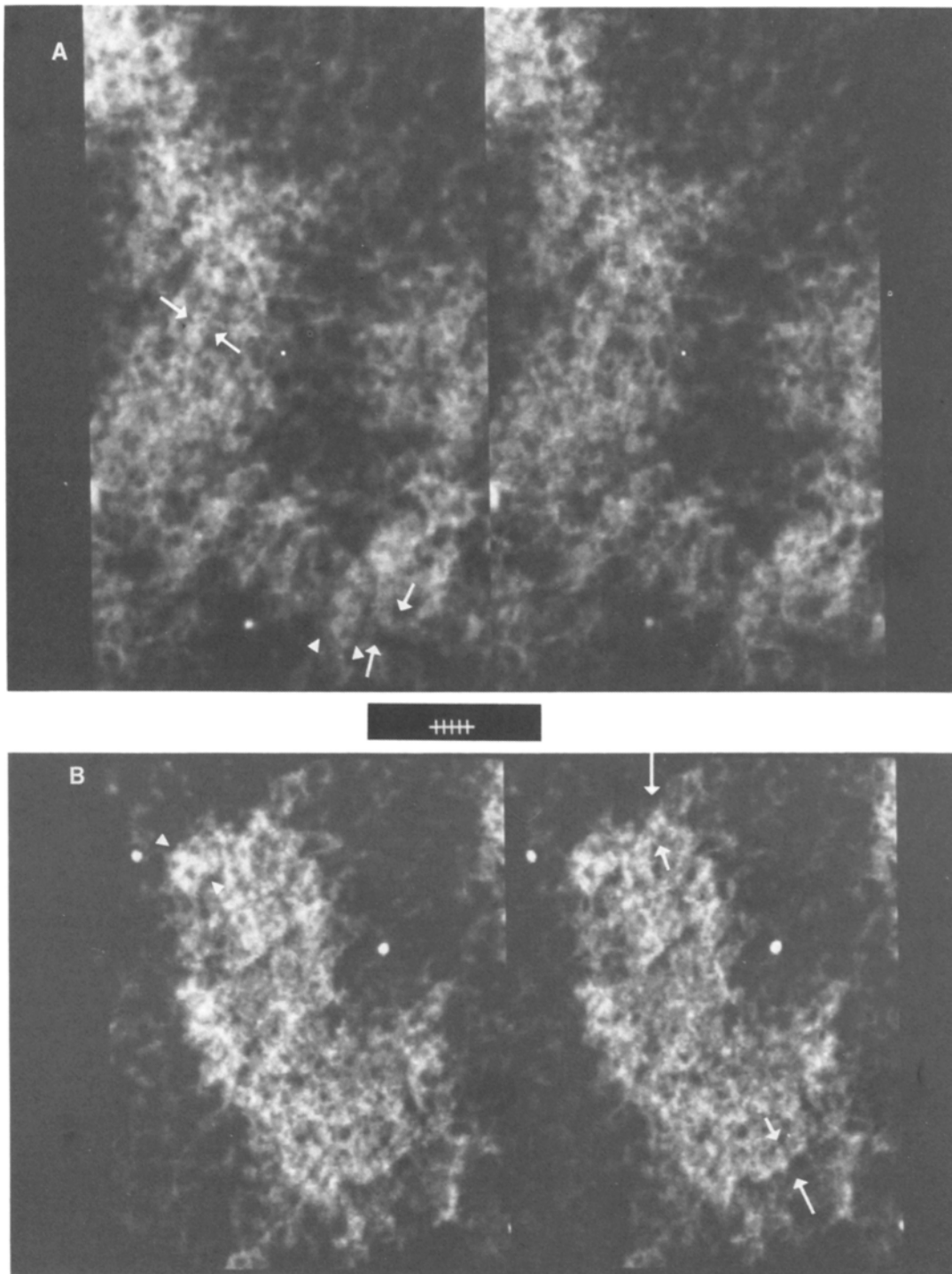
Figure 6. Two regions, shown as stereopairs, from an ∼1,500-Å Epon section of an anaphase mitotic plate contained within a precellular blastoderm *Drosophila* embryo. (*A*) A roughly longitudinal chromosome section; (*B*) an oblique chromosome section for which an axial tomography reconstruction was calculated (see Fig.7). *Arrows* mark ∼240-Å-diam fibers frequently visualized as forming folded loops or zigzags transverse to the chromosome axis. *Arrowheads* mark regions suggestive of the 400–500-Å-diam structural domains recognized in the CPD chromosomes. Crosses separated by 105 Å (5 pixels).

gle chromatids, ranged in cross section from 2,000 to 2,800 Å, and are therefore similar in diameter to the chromatids visualized within the CPD chromosomes shown in Figs. 1–3. As seen in Fig. 6, the contrast of the chromosomes within the original projected views was inferior to that obtained in the CPD chromosomes, owing to significant background staining of the nucleoplasm. Nonetheless, certain conclusions derived from the CPD syncytial blastoderm embryonic chromosomes (see above) can be further documented. Again the smallest fiber observed was roughly 120 Å in diameter,
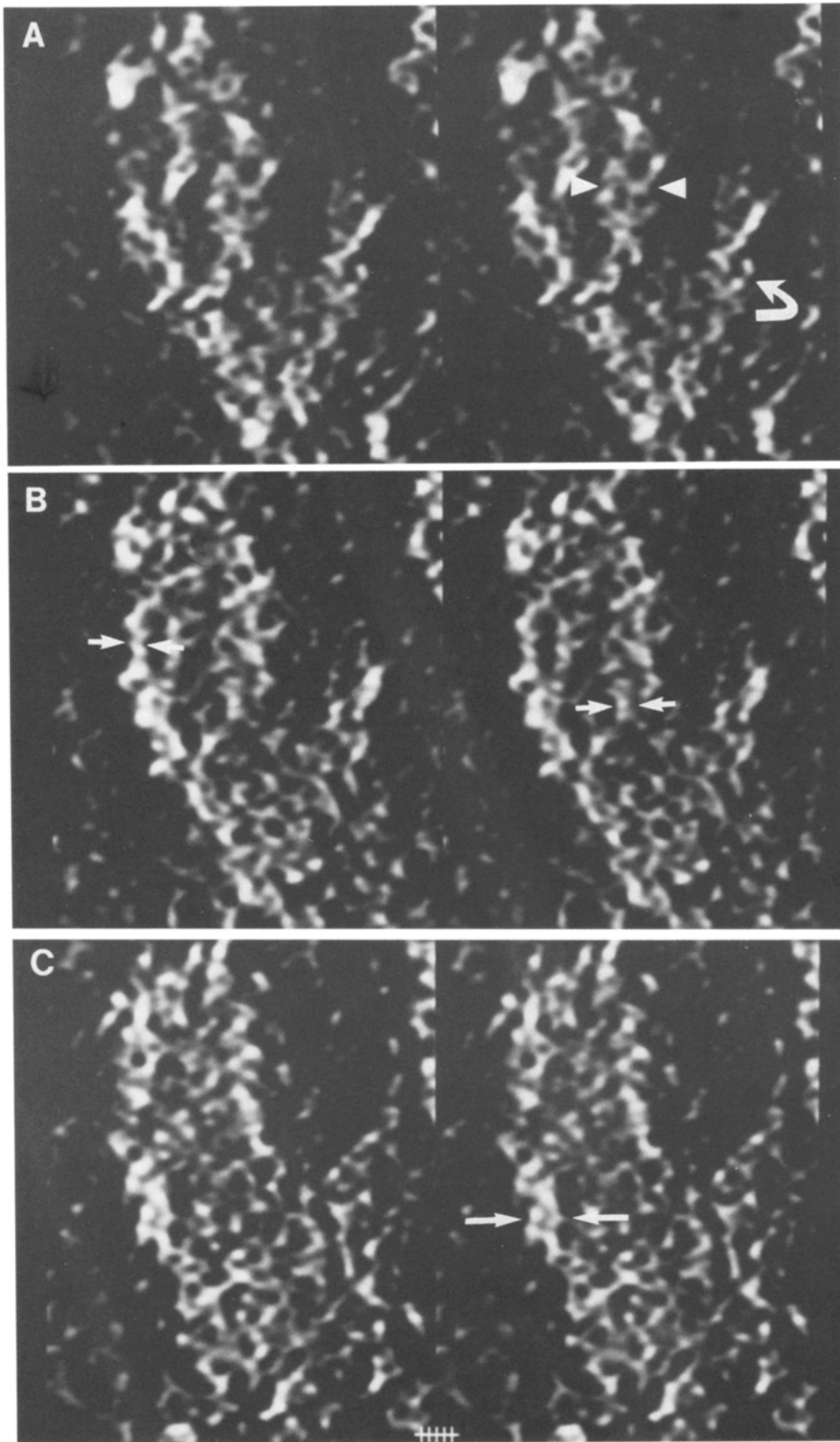
Figure 7. Stereoprojections from adjacent stacks of reconstruction slices are shown here; the axial tomography reconstruction was calculated for the chromosome region shown in Fig. 6 *B*. Each stack is 232 Å thick (11 slices). *Short arrows* (*B*) point to 240-Å fibers, *long arrows* (*C*) point to a 400–500-Å-diam structural domain. *Arrowheads* outline a region 800 Å wide, present in *A* and *B*; below it in *A* is another similar region, marked by a *curved arrow*. Crosses separated by 105 Å (5 pixels).
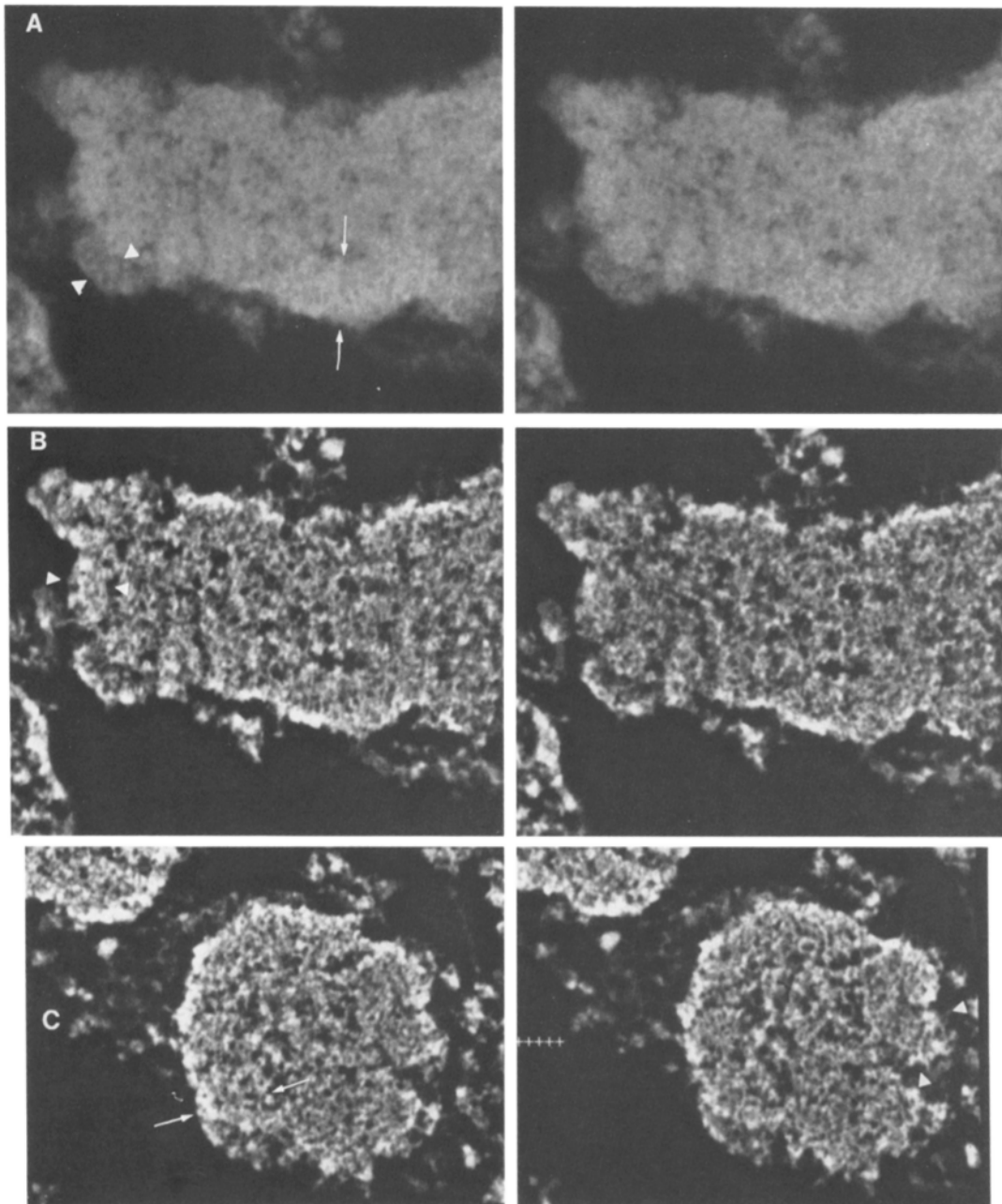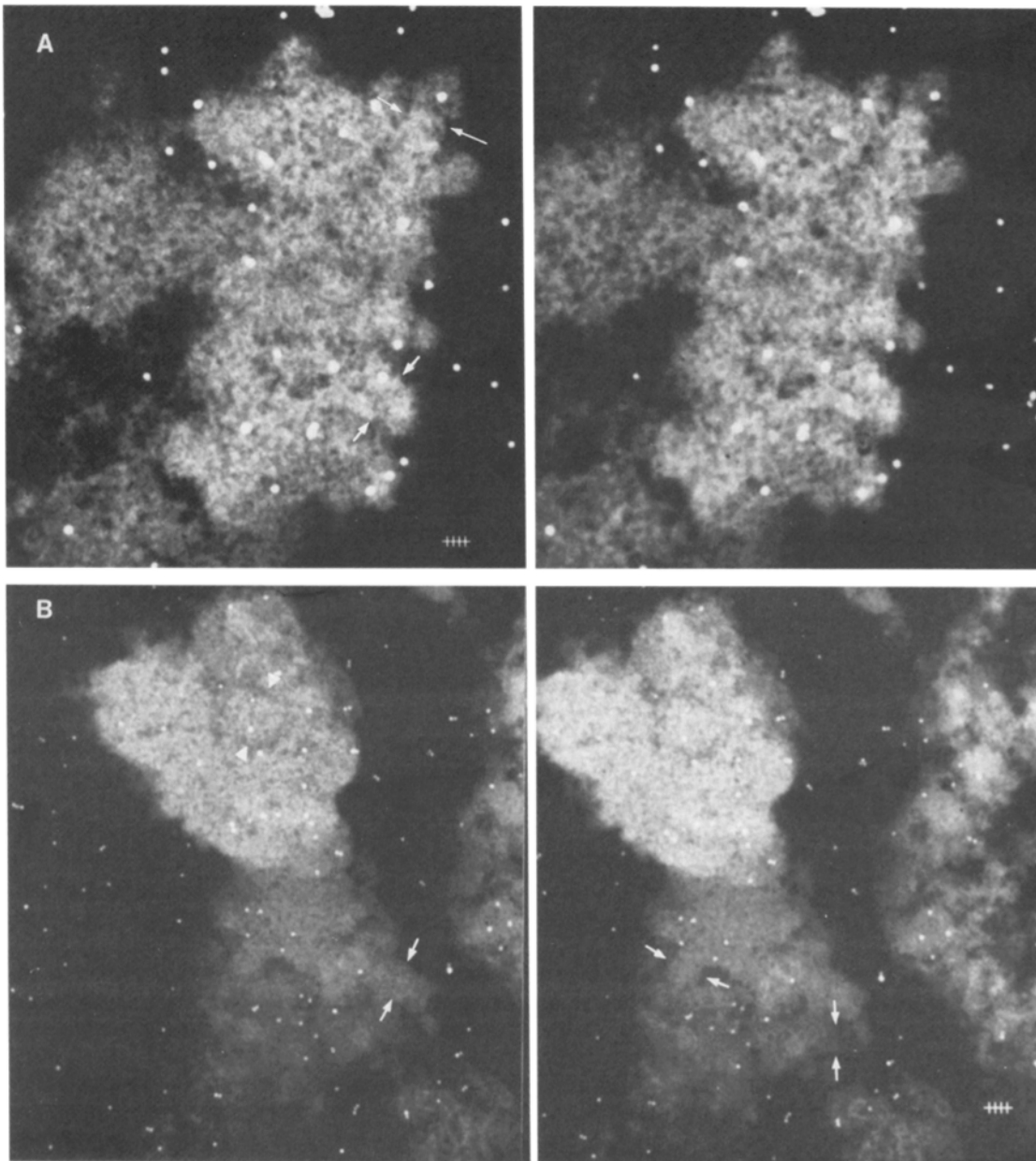
Figure 8. Stereopairs from ~2,000-Å-thick Epon sections of metaphase-arrested Kc chromosomes. (*A* and *B*) One region (from one chromatid) of a roughly longitudinal chromosome section (*A*) before and (*B*) after local contrast enhancement. *Arrowheads* (*A* and *B*) mark discrete regions of ~800 Å in diameter which are recognized in both *A* and *B*. (*C*) An approximately transverse chromosome section, contrast enhanced, in which similar 800-Å structures are recognized. In (*A–C*) structures of even larger cross-sectional diameter (1,300–1,600 Å), marked by *thin arrows*, are obvious as well. Crosses separated by 210 Å (10 pixels).

and was present largely as a component of larger-scale structures. As illustrated in Fig. 6, apparent fibers of 240 Å in diameter are seen (marked by *arrows*) and these are frequently visualized as forming folded loops, or zigzags transverse or diagonal to the chromosome axis.

The higher-order 400–500- and 800–1,000-Å structures were less prominent than in the CPD embryonic chromosomes. However, several areas suggestive of the 400–500-Å structural domains recognized in the CPD chromosomes, although less distinct in these anaphase embryo sections, are

marked by *arrowheads* in Fig. 6. No distinct 800–1,000-Å-diam structural domains were recognized in these sections, although it should be noted that certain regions within the roughly longitudinal chromosomal section shown in Fig. 6 are of this width, a typical finding based on results of serial sectioning (data not shown).

A reconstruction was calculated for the oblique chromosome section shown in Fig. 6 *B*. This reconstruction was computed from a data set consisting of 25 projections spaced every 5° of tilt over an angular range of ±60°. A montage

Figure 9. Stereopairs from 3000–4000-Å-thick Epon sections of metaphase arrested-Kc chromosomes. (*A*) A nearly longitudinal section of a chromatid; note the 800–1000-Å structural domains marked by *arrows*. Crosses separated by 105 Å. (*B*) This section corresponds to a nearly longitudinal section which is a grazing section for the chromosome half lying below the centromere (confirmed by adjacent section in serial sections [data not shown]). Again, note the 800–1,000-Å-diam structural domains, marked by *arrows*, prominent particularly in the grazing section chromosome region. *Arrowheads* mark region suggestive of the roughly 1300-Å-diam structural domains visualized in Figs. 8 and 10. Crosses separated by 210 Å.

of views from this reconstruction, representing stereoprojections from consecutive stacks of reconstruction sections, each stack 230 Å thick, is shown in Fig. 7.

Fig. 7 shows ∼240-Å fibers, marked by *short arrows*, and 400–500-Å structural domains marked by *long arrows*. Again, cross striations within these "fibers" are observed with comparable size and spacing to previous observations. In Fig. 7, *A* and *B*, a domain 800 Å wide is present (outlined by *arrowheads* in A), and below it in *A* is another similar 800-Å region (marked by a *curved arrow*).

Embedded Kc Cell Metaphase Chromosomes: Evidence for Very Large Scale, Higher-Order Chromatin Organization

The precellular blastoderm anaphase chromosomes described above showed the same structural features as the precellular blastoderm CPD mitotic chromosomes, although there appeared to be a reduced overall level of chromatin condensation. This was attributed to the accelerated cell cycle in these early embryos (mid S-phase is reached within

88
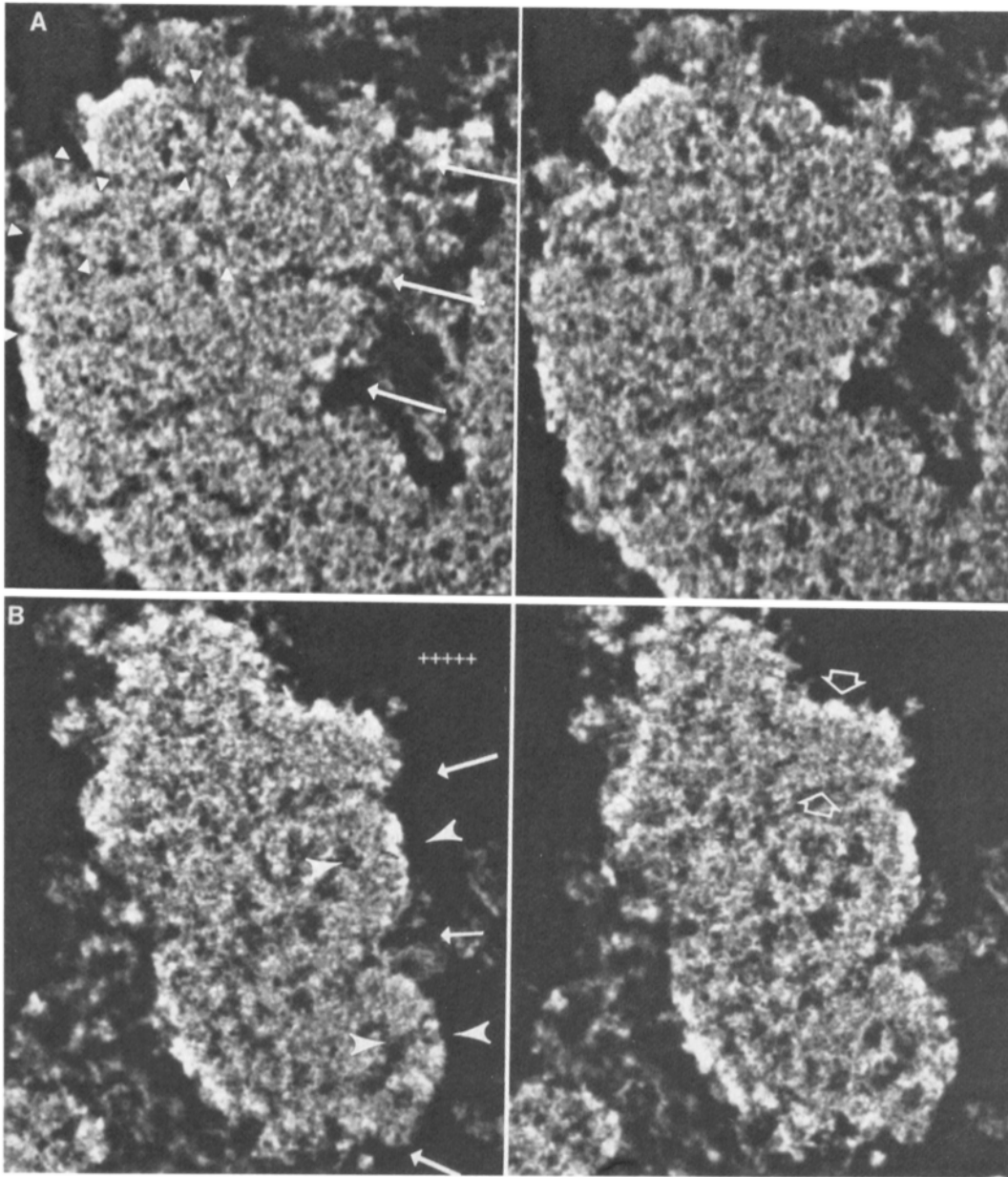
Figure 10. Stereopairs from ~2,000-Å-thick Epon sections of metaphase-arrested chromosomes. (*A*) A local contrast-enhanced region from the opposite end of the chromatid shown in Fig. 8, *A* and *B*. Suggested at the top of the panel are chromosome "bands," outlined by *small arrowheads*, measuring roughly 1,300–1,600 Å thick in this view; these create apparent contours, marked by *arrows*, 2,400–2,900 Å wide. (*B*) An oblique chromosome section; bracketed by *arrows* are two similar regions, each containing an ~800-Å-diam "fiber" (*large arrowheads*) spanning an arc roughly 2,800 Å high. Note the separation of the bottom 800-Å "fiber" into two 400-Å-diam structures. Above these regions is a roughly 1300-Å-diam structural domain, marked by *short, open arrows*. Crosses separated by 210 Å.

2–8 min after anaphase, and it is likely that the chromosomes have already begun to decondense). To analyze maximally condensed mitotic chromosomes, we used metaphase-arrested chromosomes from Kc cells, which have a distinctly higher overall level of condensation than the precellular blastoderm anaphase or mitotic chromosomes. (Although there is a possibility that the brief Colcemid treatment used to arrest these chromosomes in metaphase may have induced, at least to some degree, a nonphysiological chromosome hypercondensation, similar substructure as described be-

low was also observed in metaphase chromosomes isolated from exponentially growing cells not treated with any drugs.)

Numerous sections, varying in thickness from ~1,500 Å to >1 μm and taken from several different chromosome preparations, were examined. Typical results are shown in Figs. 8–10. Chromatids range from 0.35 to 0.8 μm in width, with the great majority varying between 0.4 and 0.6 μm. An increased overall level of chromatin condensation was observed relative to the syncytial chromosomes, with markedly increased prominence of the 800–1,000-Å structural do-

mains, as seen in Figs. 8 and 9. The smaller 400–500- and 240-Å structural entities seen previously were less commonly visible, but still well demarcated.

Within these metaphase arrested chromosomes, but not in the embryonic chromosomes described above, an even larger-scale ($\geqslant$1,000 Å) organization was observed. In Figs. 8–10, structures ("bands") measuring $\sim$1,300 Å in diameter can be visualized. Observed frequently, they are prominent features of these metaphase-arrested *Drosophila* chromosomes, as well as of human metaphase chromosomes isolated from selective detachment synchronized mitotic Hela cells (data not shown).

Finally, even larger-scale chromosomal organization, formed by the packing of the various higher-order chromatin structures described above, is suggested. In Fig. 10 *A*, chromosome "bands", outlined by *arrows* and measuring roughly 1,300–1,600 Å thick in this view, are folded at the chromosome margins to form apparent contours 2,400–2,900 Å high. Similarly, in Fig. 10 *B*, two contours roughly 2,800 Å high are outlined by the folding of 800-Å "fibers," or structural entities. (Note the separation of the lower 800-Å fiber into two $\sim$400-Å structural domains.)

Discussion

Structural Organization of Native Mitotic Chromosomes

We have described our initial findings concerning the architecture of mitotic chromosomes, derived through a three-dimensional–oriented structural approach. Using multiple projections of intact chromosomes and semithick Epon sections, obtained using both HVEM and conventional EM and combined with axial tomography and contrast-enhancement techniques, it has been possible for the first time to visualize directly significant structural detail within minimally perturbed mitotic chromosomes. Our analysis of chromosomes prepared by several different procedures, e.g., isolated CPD *Drosophila* blastoderm embryonic chromosomes, Epon sections of anaphase chromosomes from intact embedded embryos, and Epon sections of isolated metaphase-arrested chromosomes from *Drosophila* tissue culture Kc cells, shows a consistent size hierarchy of discrete chromatin structural elements, summarized in Table I. A 120-Å polynucleosomal fiber is the fundamental folding unit, which in turn is organized into higher-order structural domains. The overall organization of these domains within the mitotic chromosomes is nonsymmetric and hence, as described below, inconsistent with prevailing models of chromosome structure.

At present we cannot define the exact relationships between the various distinct levels of chromatin structural organization. We refer to the 400–500-Å "fibers" as structural domains because it is as yet unclear whether they represent a discrete higher-order fiber, formed through a continuous folding pattern of one polynucleosome chromatin fiber, as opposed to a supercoiling of either an individual or two adjacent 240-Å fibers. Similarly, the folding patterns giving rise to the 800–1,000-Å-diam structural domains observed are still unresolved. That the 240, 400–500, and 800–1,000-Å elements described in this paper do in fact represent distinct folding motifs is strongly supported by the high frequency with which they appear within several different chromosome

Table I. Summary of Results from the Three Chromosome Preparations Examined

Chromatid width (Å)	Chromosome preparation and size (Å)		
	Anaphase embryonic $\sim$2,000	CPD embryonic 2,000–2,500	Kc metaphase arrested 3,500–8,000
120	✓	✓	✓
240	++++	++	+
400–500	+	++++	++
800–1,000	+	++	++++
$\geqslant$1,300	–	–	✓

The smallest fiber observed is 120 Å in diameter. It is apparently the basic unit fiber and is seen nearly always as part of higher-order chromatin structures. The number of crosses in the tabular field corresponds to the relative prominence of particular size classes of structural domains within a given preparation. The 240-Å-diam fiber is seen in all preparations but is most prominent in the anaphase chromosomes from the embedded embryo preparation. In contrast, in the CPD chromosomes, the most prominent feature is the 400–500-Å-diam structural domain, although it too is seen in the other preparations; the 800–1,000-Å structural domain is most prominent in the metaphase-arrested chromosomes from Kc *Drosophila* tissue culture cells. Larger-scale organization is visualized only in the fully condensed metaphase-arrested Kc chromosomes. Chromatid widths vary as indicated above.

preparations of varying levels of condensation. Higher-resolution axial tomography reconstructions now in progress, in which the path of the component chromatin fibers constituting these larger-scale domains can be followed in three dimensions, should resolve the exact nature of these 400–500- and 800–1,000-Å elements, as well as of the very large 1,300-Å-diam structures seen in the fully condensed, metaphase-arrested Kc chromosomes.

The correlation between the level of chromosome condensation and the relative frequency of appearance of higher-order chromatin structures observed in the three chromosome preparations examined, summarized in Table I, strongly implies that the folding of chromatin into a fully condensed metaphase chromosome need not be viewed as a strictly sequential process, in which chromatin is first assembled into stable lower levels of organization, which, once formed, allow further compaction by subsequent higher-order folding. Instead our findings suggest that the large-scale folding of mitotic chromosomes may occur simultaneously with increased condensation, or even reorganization, at lower structural levels. Therefore a complete analysis of metaphase chromosome structure will most likely require parallel investigation of chromosome structure at several mitotic stages.

Comparison of Results with Previous Models of Chromosome Structure

In the past, many models of chromosome structure have been suggested. Currently, two of these models, mutually contradictory, have gained precedence in the literature. The first, the radial loop model (1, 9, 19, 25), postulates the existence of a nonhistone protein core or "scaffolding" serving to anchor radially oriented loops of 300-Å, quaternary chromatin fibers. While the arrangement of these loops about the scaffolding core may form distinct patterns, helical or otherwise, no higher-order discrete chromatin organization above the level of the 300-Å fiber exists within this model.

Our results on native mitotic chromosomes contradict this notion and instead indicate a hierarchy of higher-order chromatin-folding patterns >300 Å in size (400–500, 800–1,000, ∼1,300 Å). Although a looping architecture of the 249- or 400–500-Å chromatin "fibers" is prominent within the 2,000–3,000-Å-diam CPD or anaphase embryonic chromatids, these loops were not observed to be consistently oriented radially in three-dimensions about any given axis, and no evidence for a central scaffolding was indicated. The intrachromatid organization of the 800–1,000-Å-diam structural domains in all preparations studied, and the ∼1300-Å-diam domains in the highly condensed Kc metaphase arrested chromatids, are also inconsistent with a simple radial loop organization.

Our results, therefore, while not ruling out an important role for nonhistone "scaffolding" proteins serving to anchor local loops or domains of chromatin structure, do rule out a strict radial symmetry or central axis for such loops, suggesting instead a relatively diffuse organization of such proteins, if present. This conclusion is consistent with the recently observed chromosome staining (8) of antibody directed against topoisomerase II, a "scaffolding" protein. In the swollen chromosomes examined, the antibody staining was localized within separate 1,200–2,000-Å islands distributed over a central chromatid region of roughly 0.5–1.0-µm diam (presumably not significantly different from the width of the native chromatid).

In our hands, by manipulating buffer conditions while keeping all other parameters in our chromosome isolation procedure constant, we have been able to reproduce slightly swollen, "radial loop" appearing chromosomes (data not shown). Under these conditions polytene chromosomes rapidly lose structural order as observed by polarized birefringence. We are now in the process of determining the exact architecture of these chromosomes and the relationship, if any, of this architecture to that of the more native chromosomes described in this paper.

The second prominent model of chromosome structure postulates that the folding of chromosomes is based on successive helical coiling of the 300-Å fiber into a strand ∼2,000 Å in diameter, which is itself helically wound into the final metaphase chromatid structure (4, 31). Although we do observe a size hierarchy of large-scale chromatin organization, the nonsymmetric intrachromatid orientation of these higher-order structures is also incompatible with a simple form of this hierarchical helical model.

A third, related model (28) attempts to combine aspects of the above two models by suggesting a 2,000–3,000-Å radial loop structure is helically folded to form the final chromatid. While a synthesis of the two models is indeed reasonable, our data are incompatible with the proposal that the underlying 2,000–3,000-Å-diam structure is organized in a simple radial loop manner. Because the majority of our work has focused on less condensed chromatids that have a diameter of 2,000–2,500 Å, we do not yet have sufficient data pertaining to the highest level of organization in metaphase-arrested chromosomes to determine whether this organization is helical.

In conclusion, our results indicate a hierarchy of higher-order chromatin structures existing in mitotic chromosomes. The intrachromosomal arrangement of these higher-order structures does not follow predictions of either the simple radial loop or the sequential helical coiling models. Rather, our results, showing large-scale organization extending over a 0.24–0.30-µm range in metaphase-arrested chromosomes, support a model in which these higher-order chromatin structures are arranged according to a defined, nonrandom, yet complex architecture.

Apart from the results summarized above, a major conclusion from this work is the feasibility and potential for structural analysis of complex biological specimens offered by the image enhancement and axial tomography techniques discussed in this paper. When we began this work it was unclear whether the radiation damage incurred during the multiple exposures required of a tomographic approach would preclude a valid reconstruction. Our conclusion that such three-dimensional reconstructions are feasible is consistent with the conclusions of other investigators using similar techniques (24, 34, 36), and we believe this approach is generally applicable to many areas of cell biology research.

The work presented here demonstrates that unextracted, fully compacted chromosomes can be analyzed by direct structural approaches to elucidate chromosome architecture. Higher-resolution reconstructions based on an increase in angular range and sampling frequency are now in progress. Furthermore, we note that in comparison to the highly condensed mitotic chromosomes, given an adequate chromatin-specific stain for the electron microscope, the structure of interphase chromosomes should be relatively easily approached using these same methods.

References

1. Adolph, K. W. 1980. Organization of chromosomes in mitotic Hela cells. *Exp. Cell Res.* 125:95–103.
2. Agard, D. A., and R. M. Stroud. 1982. Linking regions between helices in bacteriorhodopsin revealed. *Biophys. J.* 37:589–602.
3. Athoy, B. D., S. P. Williams, and J. P. Langmore. 1985. Chromatin fibers are left-handed helices with mass per length dependent on linker length. *J. Cell Biol.* 101:2(Abstr.)
4. Bak, A. L., and J. Zeuthen. 1978. Higher order structure of mitotic chromosomes. *Cold Spring Harbor Symp. Quant. Biol.* 42:367–377.
5. Bak, A. L., J. Zeuthen, and F. H. C. Crick. 1977. Higher order structure of human mitotic chromosomes. *Proc. Natl. Acad. Sci. USA.* 74:1595–1599.
6. Blumenthal, A. B., J. D. Dieden, L. N. Kapp, and J. W. Sedat. 1979. Rapid isolation of metaphase chromosomes containing high molecular weight DNA. *J. Cell Biol.* 81:255–259.
7. Daskal, Y., M. L. Mace, W. Wray, and H. Busch. 1976. Use of direct current sputtering for improved visualization of chromosome topology by scanning electron microscopy. *Exp. Cell Res.* 100:204–212.
8. Earnshaw, W. C., and M. M. S. Heck. 1985. Localization of topoisomerase 2 in mitotic chromosomes. *J. Cell Biol.* 100:1716–1725.
9. Earnshaw, W. C., and U. K. Laemmli. 1983. Architecture of metaphase chromosomes and chromosome scaffolds. *J. Cell Biol.* 96:84–93.
10. Elgin, S. C. R., and D. W. Miller. 1978. Mass rearing of flies and mass production and harvesting of embryos. *In* The Genetics and Biology of *Drosophila.* Vol. 2A. (M. Ashburner and T. R. F. Wright, editors. Academic Press, Inc., London. 112–120.
11. Foe, V. E., and B. M. Alberts. 1983. Studies of nuclear and cytoplasmic

behavior during the five mitotic cycles that precede gastrulation in *Drosophila* embryogenesis. *J. Cell Sci.* 61:31–70.

12. Glaeser, R. M. 1982. A critique of the theoretical basis for the use of HVEM in biology. Proceedings of the 40th Annual Meeting, Electron Microscopy Society of America. G. W. Bailey, editor. Claitor's Publishing Division, Baton Rouge, LA. 2–3.

13. Gorden, R., and G. T. Herman. 1974. Three-dimensional reconstruction from projections: a review of algorithms. *Int. Rev. Cytol.* 38:111–151.

14. Harrison, C. J., T. D. Allen, M. Britch, and R. Harris. 1982. High-resolution scanning electron microscopy of human metaphase chromosomes. *J. Cell Sci.* 56:409–422.

15. Hayat, M. A. 1981. Principles and Techniques of Electron Microscopy-Biological Applications. Vol. 1, 2nd edition. University Park Press, Baltimore. 161.

16. Iino, A. 1971. Observations on human somatic chromosomes treated with hyaluronidase. *Cytogenetics (Basel).* 10:286–294.

17. Klug, A., and R. A. Crowther. 1972. Three-dimensional image reconstruction from the viewpoint of information theory. *Nature (Lond.).* 238:435–440.

18. Lawrence, M. C. 1983. Alignment of images for three-dimensional reconstruction of non-periodic objects. *Electron Microsc. Soc. South. Afr. Proc.* 13:19–20.

19. Marsden, M. P. F., and U. K. Laemmli. 1979. Metaphase chromosome structure: evidence for a radial loop model. *Cell.* 17:849–858.

20. Mullinger, A. M., and R. T. Johnson. 1980. Packing DNA into chromosomes. *J. Cell Sci.* 46:61–86.

21. Mullinger, A. M., and R. T. Johnson. 1983. Units of chromosome replication and packing. *J. Cell Sci.* 64:179–193.

22. Ohnuki, Y. 1968. Structure of chromosomes. 1. Morphological studies of the spiral structure of human somatic chromosomes. *Chromosoma (Berl.).* 25:402–428.

23. Okada, T. A., and D. E. Comings. 1979. Higher order structure of chromosomes. *Chromosoma (Berl.).* 72:1–14.

24. Olins, A. L., D. E. Olins, H. A. Levy, R. C. Durfee, S. M. Margle, E. P. Tinnel, B. E. Hingerty, S. D. Dover, and H. Fuchs. 1984. Modeling Balbiani ring gene transcription with electron microscope tomography. *Eur. J. Cell Biol.* 35:129–142.

25. Paulson, J. R., and U. K. Laemmli. 1977. The structure of histone depleted chromosomes. *Cell.* 12:817–828.

26. Peii, T., and J. S. Lim. 1982. Adaptive filtering for image enhancement.

27. Ramachandran, G. N., and A. V. Lakshminarayanan. 1971. Three-dimensional reconstruction from radiographs and electron micrographs: application of convolutions instead of Fourier transforms. *Proc. Natl. Acad. Sci. USA.* 68:2236–2240.

28. Rattner, J. B., and C. C. Lin. 1985. Radial loops and helical coils coexist in metaphase chromosomes. *Cell.* 42:291–296.

29. Ris, H. 1981. Stereoscopic electron microscopy of chromosomes. *Methods Cell Biol.* 22:77–96.

30. Ross, M. J., and R. M. Stroud. 1977. Error analysis in the biophysical applications of a flatbed autodensitometer. *Acta Crystallogr.* A33:500–508.

31. Sedat, J., and L. Manuelidis. 1978. A direct approach to the structure of eukaryotic chromosomes. *Cold Spring Harbor Symp. Quant. Biol.* 42:331–350.

32. Skaer, R. J., and S. Whytock. 1976. The fixation of nuclei and chromosomes. *J. Cell Sci.* 20:221–231.

33. Skaer, R. J., and S. Whytock. 1977. Chromatin-like artifacts from nuclear sap. *J. Cell Sci.* 26:301–310.

34. Skoglund, U. K., K. Andersson, B. Strandberg, and B. Daneholt. 1986. Three-dimensional structure of a specific pre-messenger RNP particle established by electron microscope tomography. *Nature (Lond.).* 319:560–564.

35. Stubblefield, E., and W. Wray. 1971. Architecture of the chinese hamster metaphase chromosome. *Chromosoma (Berl.).* 32:262–294.

36. Subirana, J. A., S. M. Munoz-Guerra, J. Aymami, M. Radermacher, and J. Frank. 1985. The layered organization of nucleosomes in 30 nm chromatin fibers. *Chromosoma (Berl.).* 91:377–390.

37. Turkevich, J., P. C. Stevenson, and J. Hillier. 1953. The formation of colloidal gold. *J. Phys. Chem.* 57:670–673.

38. Utsumi, K. R., and Tanaka, T. 1975. Studies on the structure of chromosomes. 1. The uncoiling of chromosomes revealed by treatment with hypotonic solution. *Cell Struct. Funct.* 1:93–99.

39. Woodcock, C. L. F., L. L. Y. Frodo, and J. B. Rattner. 1984. The higher order structure of chromatin: evidence for a helical ribbon arrangement. *J. Cell Biol.* 99:42–52.

40. Zalokar, M., and I. Erk. 1977. Phase-partition fixation and staining of *Drosophila* eggs. *Stain Technol.* 52:89–95.

41. Zatsepina, O. V., V. Y. Polyakov, and Y. S. Chentsov. 1983. Chromonema and chromomore: structural units of mitotic and interphase chromosomes. *Chromosoma (Berl.).* 88:91–97.

Opt. Eng. 21:108–112.